Photoelectron Spectroscopic and Theoretical Study of Aromatics−Pb_m Anionic Complexes (Aromatics = C_6H_5, C_5H_4N, C_4H_3O, and C_4H_4N; $m = 1-4$): A Comparative Study

Zhang Sun, Shutao Sun, Hongtao Liu, Qihe Zhu, and Zhen Gao*

Beijing National Laboratory for Molecular Sciences (BNLMS), State Key Laboratory of Molecular Reaction Dynamics, Center of Molecular Science, Institute of Chemistry, Chinese Academy of Sciences, Beijing 100080, People's Republic of China

Zichao Tang†

Beijing National Laboratory for Molecular Sciences (BNLMS), State Key Laboratory of Molecular Reaction Dynamics, Center of Molecular Science, Institute of Chemistry, Chinese Academy of Sciences, Beijing 100080, People's Republic of China, and State Key Laboratory of Molecular Reaction Dynamics, Dalian Institute of Chemical Physics, Chinese Academy of Sciences, Dalian 116023, People's Republic of China

Received: July 2, 2008; Revised Manuscript Received: September 8, 2008

The reactions between lead vapored by laser ablation and different aromatic molecules (C_6H_6, C_5H_5N, C_4H_4O, or C_4H_5N) seeded in argon carrier gas were studied by a reflectron time-of-flight mass spectrometer (RTOF-MS) with a photoelectron spectrometer. The adiabatic electron affinities (EAs) of the dominant anionic products $Pb_mC_6H_5^-$, $Pb_mC_5H_4N^-$ ($m = 1-4$) and $Pb_mC_4H_3O^-$, $Pb_mC_4H_4N^-$ ($m = 1-3$) dehydrogenated complexes are obtained from the photoelectron spectra with 308 and 193 nm photon, respectively. It is found that the EAs of $Pb_mC_4H_4N$ are higher than those of $Pb_mC_6H_5$, $Pb_mC_5H_4N$, and $Pb_mC_4H_3O$ with the same metal number m. The possible structures for $Pb_mC_4H_4N^-$ complexes were calculated with density functional theory (DFT) and the most stable structure was confirmed. The adiabatic detachment energies for the most stable structure were in agreement with the experimental PES results. The calculated density of state (DOS) agrees with the experimental PES spectrum well. It was confirmed by the theoretical calculations that the C_4H_4N group bonds on lead clusters through the Pb−N σ bond.

1. Introduction

The interaction of metals with organic molecules is of fundamental interest to chemical and material science. In recent years, many experimental[1−14] and theoretical[15−28] investigations on the interaction of metal clusters with benzene in the gas phase have been extensively reported. Furthermore, some studies of [$M_m$phenyl]$^-$ complexes were also reported. Xing et al.[29] reported the generation of [$M_m$phenyl]$^-$ (M = Mn−Cu) complexes. The phenyl−coinage metal complexes ($Ag_mC_6H_5^-$, $Au_mC_6H_5^-$, $m = 1-3$)[30] and phenyl−lead metal complexes ($Pb_mC_6H_5^-$, $m = 1-5$)[31] were studied by photoelectron spectroscopy (PES) and density functional theory (DFT). While these studies focus mainly on the reaction of metal species with the benzene molecule, the research is still required on the reactions of main group metal clusters with other aromatic molecules.

Lead is the heaviest element in group IV. It is known that the bulk lead solid is metallic, in contrast to the semiconductors of silicon and germanium crystals. The structure of lead clusters is intriguing among the clusters of group IV, due to its large relativistic effects and especially spin−orbit coupling.[32,33] As early as 1972, Castleman and co-workers[34] studied the gas-phase hydration of the monovalent lead ion using high-pressure mass spectrometry, and clusters of up to eight water molecules around a single lead ion were observed. Later the same group reported the clustering reaction of benzene with lead ions, and reported that Pb^+−benzene displayed an unusually strong interaction.[35] In our publications,[4] the reactions of lead cluster anions with benzene have been reported. The important intermediate series of products were [Pb_m−phenyl]$^-$ ($m = 1-5$), which were rare cases in chemistry.

Aromatic molecules, especially heterocyclic aromatic molecules, are one part of the most important organic molecules in chemistry and biology. The study on heterocyclic aromatic molecules is of great significance in biochemistry and pharmacy.[36,37] Furan and pyrrole are five-membered heterocycles, and are prone to electrophilic substitution. The studies of these molecules[38,39] have been reported. The C−H and N−H activations of aromatic compounds were studied experimentally[40] and theoretically.[41,42] It has been shown that the N−H bond activation is both kinetically and thermodynamically preferred to C−H activation.

Here we report a study, by mass spectrum and PES, on $Pb_mC_6H_5^-$, $Pb_mC_5H_4N^-$ ($m = 1-4$) and $Pb_mC_4H_3O^-$, $Pb_mC_4H_4N^-$ ($m = 1-3$) dehydrogenated complexes, which were produced from reactions between aromatic molecules (C_6H_6, C_5H_5N, C_4H_4O, or C_4H_5N) and lead vapor generated by laser ablation on lead solid sample. By combination of experimental and theoretical studies, we have obtained some important information about the bonding and geometric and electronic structures of the $Pb_mC_4H_4N^-$ complexes.

2. Experimental Methods

The apparatus used in the experiments mainly consists of a homemade reflectron time-of-flight mass spectrometer (RTOF-MS) and a photoelectron spectrometer with magnetic-bottle-type analyzer. The details of the apparatus have been described elsewhere,[43,44] and only an outline is given below.

* Address correspondence to this author. E-mail: gaoz@iccas.ac.cn.
† E-mail: zctang@dicp.ac.cn.

10.1021/jp805837b CCC: $40.75
Published on Web 10/23/2008

A rotating lead disk target (purity >99.99%) in the source chamber of RTOF-MS was ablated by a pulsed laser beam (1064 or 532 nm Nd:YAG laser, 5 Hz, ~10 mJ/pulse). The laser-induced plasma was carried by molecular beam generated with a pulsed valve at a backing pressure of about 400 kPa of argon (purity 99.99%), seeded with C_6H_6, C_5H_5N, C_4H_4O, or C_4H_5N, respectively. The ratio of aromatic molecules in the mixed gas is about 0.1% by volume. The aromatics−Pb_m anionic products from the reactions of Pb plasma and aromatic molecules are entrained by the carrier gas and undergo low pressure (10^{-2} Pa) expansion in the source chamber. After passing a skimmer, all products enter into the acceleration area in the spectroscopic chamber of RTOF-MS (10^{-4} Pa). The anionic clusters are accelerated in the direction perpendicular to the molecular beam and then are reflected toward the detector, double microchannel plates (MCP). The resolution ($M/\Delta M$) of RTOFMS is better than 2000, so it is easy to resolve the number of hydrogen atoms in the products.

The anionic products can be mass selected by the timing probe and are photodetached by an excimer laser (XeCl 308 nm or ArF 193 nm). The photoelectrons detached are measured by the photoelectron spectrometer, a magnetic-bottle time-of-flight analyzer. The PES spectrum is calibrated by the known spectra of Cu^-, Ag^-, and Au^-. The energy resolution of the photoelectrons is about 70 meV for electrons with 1 eV kinetic energy.

3. Computational Methods

The geometric optimization for all possible structures of the products was performed with relativistic density functional calculations at the level of generalized gradient approach, using a Perdew−Wang exchange-correlation functional.[45] The zero-order regular approximation Hamiltonian was used to account for the scalar (mass velocity, Darwin, and spin−orbit) relativistic effects.[46] The standard Slater-type orbital basis sets of the triple-ζ plus two polarization functions (TZ2P) were used for the orbitals of Pb, C, N, O, and H atoms. And the frozen core ($1s^2-4f^{14}$) approximation was used for Pb. All the calculations were accomplished with the Amsterdam density functional (ADF 2005)[47] programs. It has been indicated that these theoretical methods are suitable for study on the metal clusters.[19,48,49]

4. Results and Discussion

4.1. Mass Spectrum. Figure 1 shows the typical mass spectra of the anionic products generated from the reactions between lead vapor generated by laser ablation and different aromatic molecules (a: C_6H_6; b: C_5H_5N; c: C_4H_4O; d: C_4H_5N) seeded in argon carrier gas. All the mass spectra were calibrated carefully according to the mass numbers of pure metal clusters. The enlarged parts in Figure 1 show the mass spectra of the isotope of Pb_3^-, which can be resolved clearly. So the resolution of the mass spectrometer is enough to assign the products correctly and to resolve the hydrogen distribution.

As shown in Figure 1, the dominant anionic products of the reactions between Pb with C_6H_6, C_5H_5N, C_4H_4O, and C_4H_5N respectively are $Pb_mC_6H_5^-$ ($m = 1-4$), $Pb_mC_5H_4N^-$ ($m = 1-6$), $Pb_mC_4H_3O^-$ ($m = 1-5$), and $Pb_mC_4H_4N^-$ ($m = 1-4$) dehydrogenated complexes. The formation mechanism of the $Pb_mC_6H_5^-$ complexes has been discussed in detail in ref 4, shown as follows

$$Pb_m^- + C_6H_6 \rightarrow [Pb_m \cdots (C_6H_6)]^{-\cdot} \xrightarrow{Ar} Pb_mC_6H_5^- + H \quad (1)$$

It involves the selective C−H cleavage of benzene due to the negative charge and the excessive energy in metal clusters. Here, we assume that the formation mechanisms of $Pb_mC_5H_4N^-$, $Pb_mC_4H_3O^-$, and $Pb_mC_4H_4N^-$ are similar to that of $Pb_mC_6H_5^-$ due to the same reaction conditions for the same kind of reactants

4.2. PES Spectra with 308 and 193 nm Photon. The photoelectron spectra of $Pb_mC_6H_5^-$, $Pb_mC_5H_4N^-$ ($m = 1-4$) and $Pb_mC_4H_3O^-$, $Pb_mC_4H_4N^-$ ($m = 1-3$) at 308 nm (4.03 eV) photon are shown in Figure 2. As shown in Figure 2, the evaluated EA of the corresponding complexes is indicated with the arrow. The evaluation has considered the instrumental resolution (70 meV/1 eV). There are some weak bands in some PES spectra, for example, those of $Pb_3C_6H_5^-$, $Pb_4C_6H_5^-$, $Pb_2C_4H_4N^-$, and $Pb_3C_4H_4N^-$. They might be caused by the isomers of these complexes or the little contamination from the spectrometer cavity. From Figure 2, we can see that the EAs of $Pb_mC_6H_5$, $Pb_mC_5H_4N$ ($m = 1-4$) and $Pb_mC_4H_3O$, $Pb_mC_4H_4N$ ($m = 1-3$) increase with the increase of Pb atom number. This tendency can be explained by the effective core potential. These complexes are all the closed-shell electron system. So the more metal atoms these complexes contain, the stronger the effective core potential of the outer electron in the metal cluster will feel, and so the EA increases.

The photoelectron spectra of $Pb_mC_6H_5^-$, $Pb_mC_5H_4N^-$ ($m = 1-4$) and $Pb_mC_4H_3O^-$, $Pb_mC_4H_4N^-$ ($m = 1-3$) at 193 nm (6.42 eV) photon are shown in Figure 3. The photoelectron spectra at 193 nm photon can show more electronic information, because the 193 nm photon (6.42 eV) has a higher energy than the 308 nm photon (4.03 eV). But the resolution of the spectra obtained with the 193 nm photon is worse than that of the spectra at the 308 nm photon, especially for the low binding energy sides of the spectra.

Figures 2 and 3 indicate that the PES spectra of aromatics−Pb_m vary with the variety of the aromatic group. The distribution of the PES spectra for one Pb atom bonding different aromatic groups is different. As the Pb atom number increases, the distribution of the PES spectra is going to be similar. For Pb_3−aromatic, their PES spectra all present three peaks in the low bonding energy side. The PES spectra of aromatics−Pb_m indicates that the effect of the aromatic group on the Pb_m cluster becomes weak as the metal number m increases.

The affirmed electron affinities of aromatics−Pb_m (aromatics = C_6H_5, C_5H_4N, C_4H_3O, C_4H_4N, $m = 1-3$) at 308 and 193 nm photon are shown in Table 1. From Table 1, it is clear that the tendency, i.e., the EAs of $Pb_mC_6H_5$, $Pb_mC_5H_4N$, $Pb_mC_4H_3O$, and $Pb_mC_4H_4N$ ($m = 1-3$) with the same metal number m are gradually increasing. The EAs of $Pb_mC_6H_5$, $Pb_mC_5H_4N$, and $Pb_mC_4H_3O$ are very close to each other, and the difference is about 0.2 eV. However, the EAs of $Pb_mC_4H_4N$ are higher than the others, and the difference is over 0.4 eV. It has been reported that the phenyl group binds on lead clusters through the Pb−C σ bond for $Pb_mC_6H_5^-$ complexes.[31] For $Pb_mC_5H_4N^-$, $Pb_mC_4H_3O^-$ complexes, Pb clusters might replace the H atom of C_5H_5N and C_4H_4O to form dehydrogenated complexes through the Pb−C bond. However, C_4H_5N has three different H atoms, and one binds N though the N−H bond. The higher EAs of $Pb_mC_4H_4N$ might indicate that the Pb clusters bind the C_4H_4N group though the Pb−N bond, for the electronegativity of the N atom is larger than that of the C atom.[50] To confirm this point, we studied the geometric and electronic structures of $Pb_mC_4H_4N^-$ complexes by DFT calculations.

4.3. Low-Energy Structures. We considered a variety of structures for both the neutrals $Pb_mC_4H_4N$ and anions $Pb_mC_4H_4N^-$ ($m = 1-3$). The optimized possible structures are shown in Figure 4, and their structural energetic characteristics are summarized in Table 2.

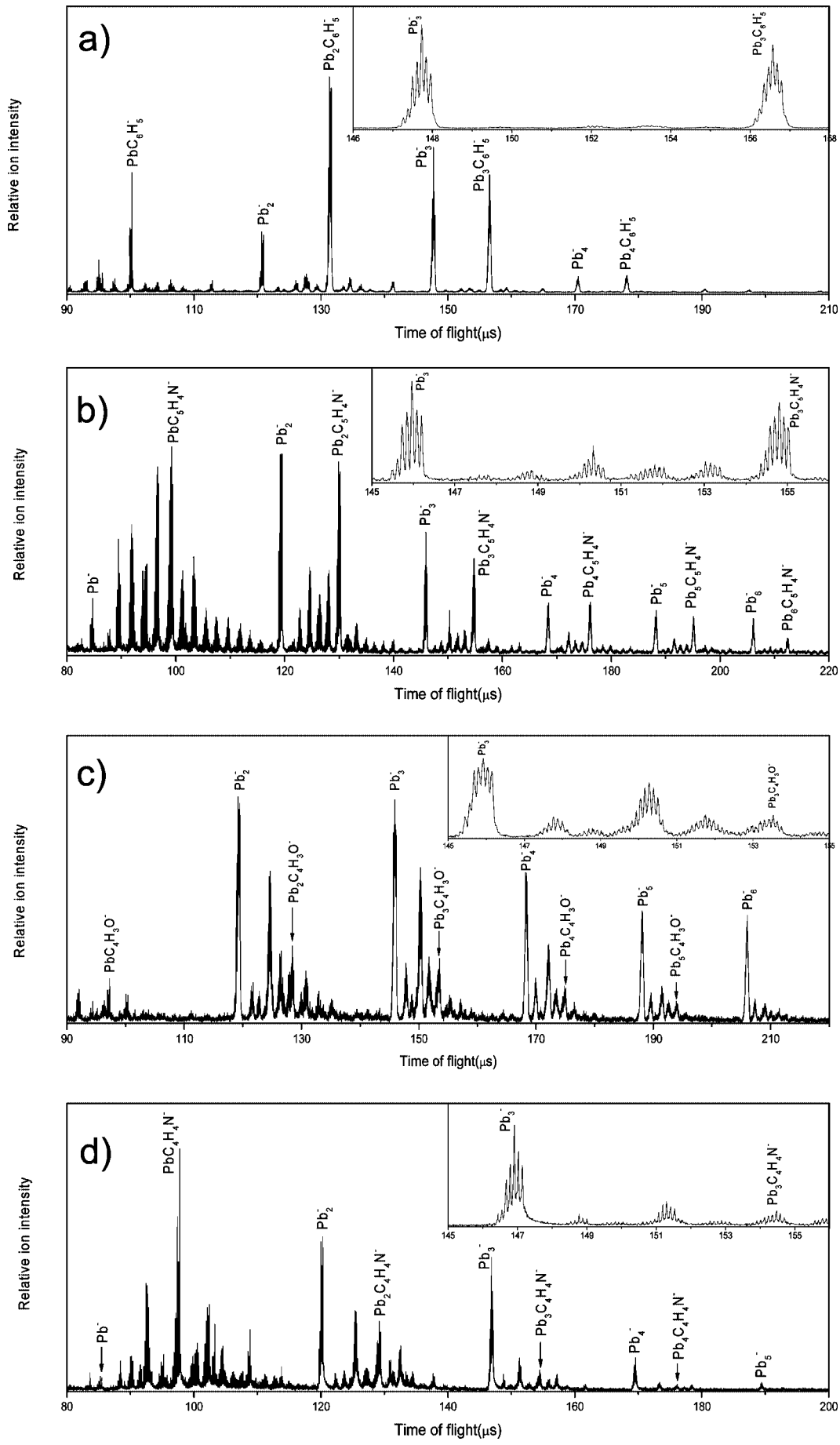

Figure 1. The measured mass spectra of the anionic products from the reactions between lead vapor generated by laser ablation and aromatic molecules (a: C_6H_6; b: C_5H_5N; c: C_4H_4O; d: C_4H_5N) seeded in argon carrier gas (0.1% aromatic molecules in 400 kPa mixed gas). The insets in the spectra show the enlarged part of the spectrum.

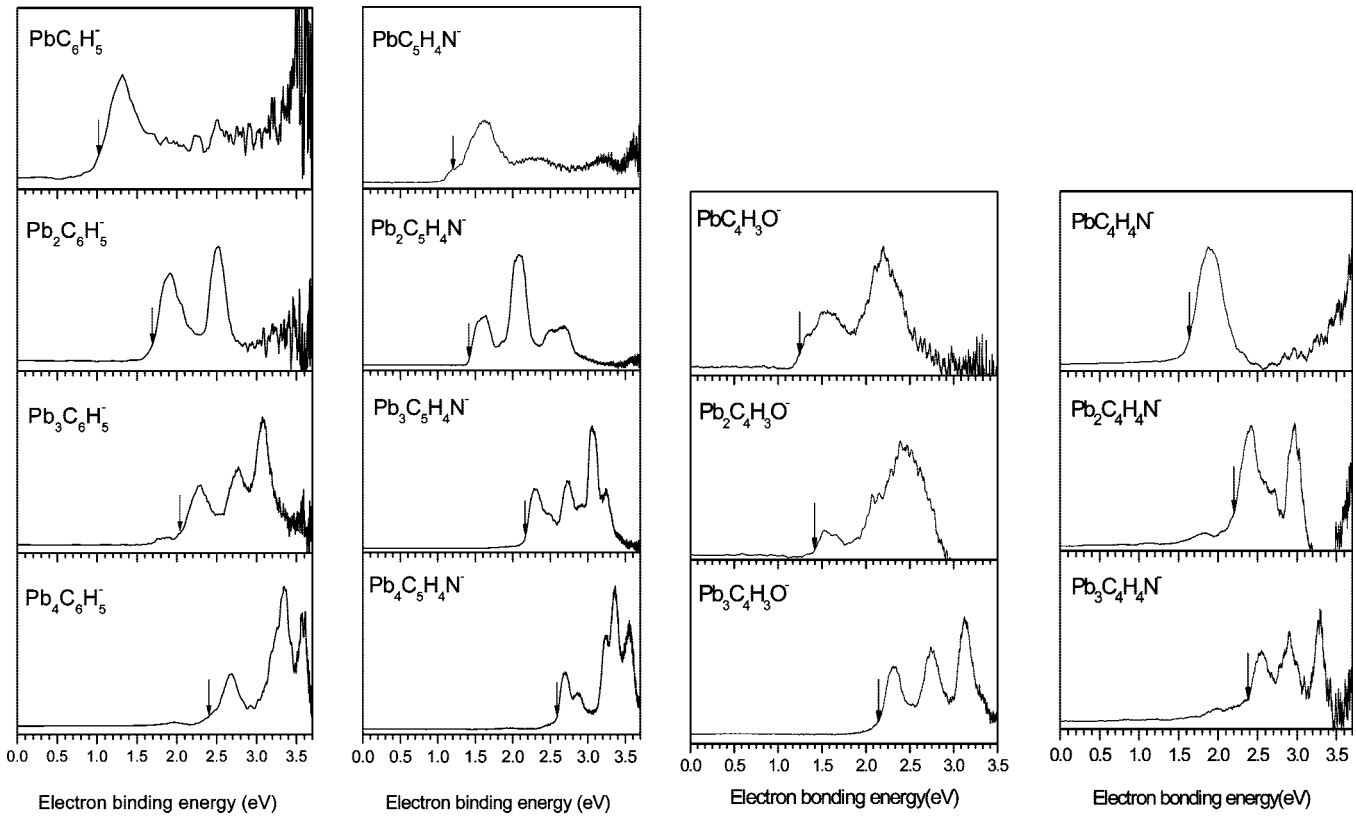

Figure 2. Photoelectron spectra of $Pb_mC_6H_5^-$, $Pb_mC_5H_4N^-$ ($m = 1-4$) and $Pb_mC_4H_3O^-$, $Pb_mC_4H_4N^-$ ($m = 1-3$) at 308 nm (4.03 eV) photon.

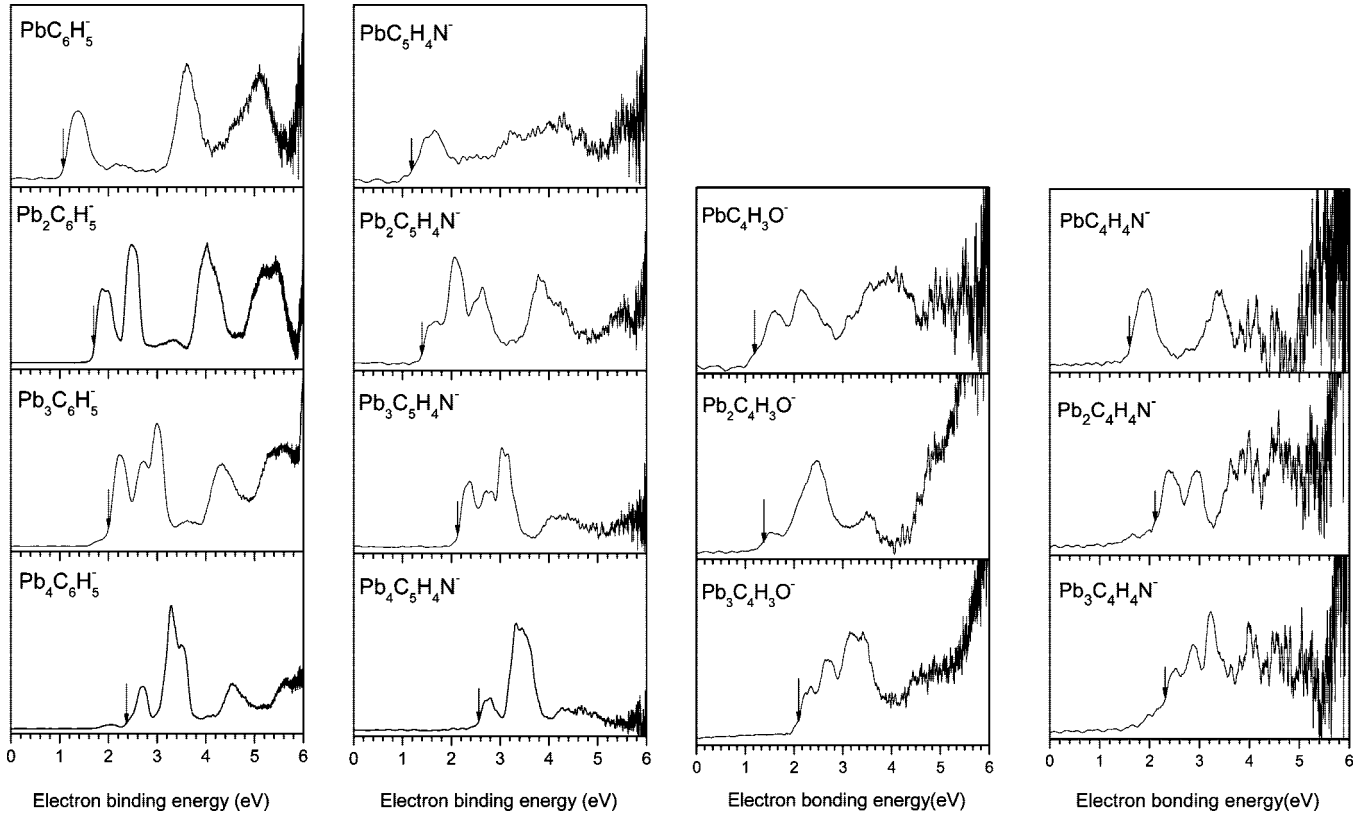

Figure 3. Photoelectron spectra of $Pb_mC_6H_5^-$, $Pb_mC_5H_4N^-$ ($m = 1-4$), and $Pb_mC_4H_3O^-$, $Pb_mC_4H_4N^-$ ($m = 1-3$) at 193 nm (6.42 eV) photon.

For the $PbC_4H_4N^-$ anion, the lowest energy structure is C_{2v} symmetry with a $^3B_1$ state (I), in which the C_4H_4N group couples on a metal atom through an N−Pb bond. The ortho-isomer (II) and *p*ara-isomer (III) of anion $PbC_4H_4N^-$, in which the C_4H_4N group couples on a metal atom through a C−Pb bond, are 0.58 and 1.22 eV higher in energy than isomer I, respectively. For PbC_4H_4N neutral, the lowest energy structure is C_{2v} symmetry with a $^2A_2$ state (I), and the ortho-isomer (II) and para-isomer (III) of neutral PbC_4H_4N are 0.28 and 0.36 eV higher in energy than isomer I, respectively.

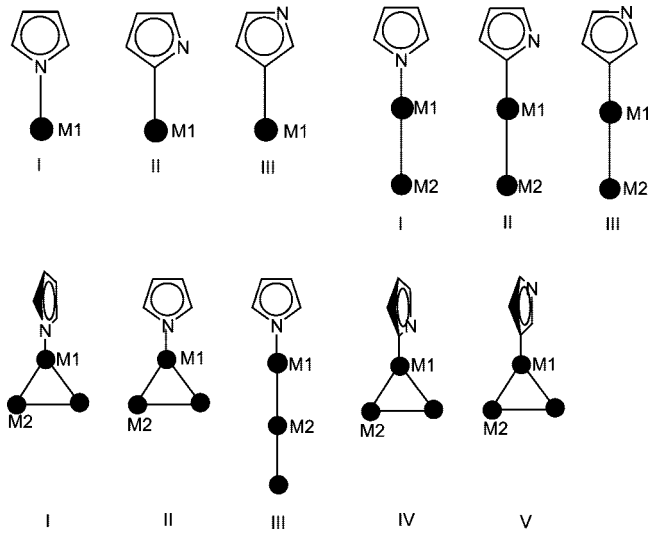

Figure 4. Optimized structures for neutrals $Pb_mC_4H_4N$ ($m = 1-3$) and anions $Pb_mC_4H_4N^-$ ($m = 1-3$). See Table 2 for structural parameters.

TABLE 1: The Measured Electron Affinities (eV) for Aromatics−Pb_m (aromatics = C_6H_5, C_5H_4N, C_4H_3O, C_4H_4N, $m = 1-3$) at 308 and193 nm Photon

	$Pb_mC_6H_5$		$Pb_mC_5H_4N$		$Pb_mC_4H_3O$		$Pb_mC_4H_4N$	
m	308 nm	193 nm	308 nm	193 nm	308 nm	193 nm	308 nm	193 nm
1	1.01	1.01	1.20	1.08	1.24	1.22	1.65	1.63
2	1.70	1.70	1.41	1.39	1.42	1.34	2.17	2.20
3	2.03	2.03	2.16	2.14	2.14	2.10	2.39	2.41

TABLE 2: Various Structural and Energetic Characteristics of Neutrals $Pb_mC_4H_4N$ ($m = 1-3$) and Anions $Pb_mC_4H_4N^-$ ($m = 1-3$)

	isomer	state	point group	$R_{N(C)-M1}$ (Å)	$\theta_{N(C)-M1-M2}$ (deg)	ΔE^a (eV)	EA (eV) calcd	EA (eV) exptl[b]
PbC_4H_4N	I	$^2A_2$	C_{2v}	2.29		0.00	1.61	1.65
	II	$^2A'$	C_s	2.32		0.28	1.22	
	III	$^2A'$	C_s	2.31		0.36	1.00	
$PbC_4H_4N^-$	I	$^3B_1$	C_{2v}	2.44		0.00		
	II	$^3A''$	C_s	2.43		0.58		
	III	$^3A''$	C_s	2.42		1.22		
$Pb_2C_4H_4N$	I		C_{2v}	2.26	180	0.10	2.26	2.21
	II	$^2A''$	C_s	2.28	180	0.06	1.90	
	III	$^2A''$	C_s	2.28	180	0.00	1.68	
$Pb_2C_4H_4N^-$	I	$^1A_1$	C_{2v}	2.35	180	0.00		
	II	$^1A'$	C_s	2.35	180	0.33		
	III	$^1A'$	C_s	2.35	180	0.48		
$Pb_3C_4H_4N$	I	$^2B_1$	C_{2v}	2.31	148.6	0.07	2.57	2.41
	II	$^2B_1$	C_{2v}	2.28	148.5	0.09	2.68	
	III	$^2B_1$	C_{2v}	2.35	180	0.88	2.53	
	IV	$^2A''$	C_s	2.29	148.5	0.08	2.16	
	V	$^2A''$	C_s	2.27	148.8	0.00	1.94	
$Pb_3C_4H_4N^-$	I	$^1A_1$	C_{2v}	2.41	145.5	0.09		
	II	$^1A_1$	C_{2v}	2.38	145.8	0.00		
	III	$^1A_1$	C_{2v}	2.61	180	0.94		
	IV	$^1A'$	C_s	2.37	146.3	0.51		
	V	$^1A'$	C_{2v}	2.38	147.6	0.65		

[a] ΔE is the difference in energy relative to the corresponding lowest lying structure. [b] The uncertainty for the experimental EA is ±0.035 eV.

For anion $Pb_2C_4H_4N^-$, the lowest energy structure is C_{2v} symmetry (I), in which the C_4H_4N group couples on a metal atom through an N−Pb bond. This structure is similar to the structure of $Pb_2C_6H_5$.[31] The ortho-isomer (II) and para-isomer (III) of the anion $Pb_2C_4H_4N^-$, in which the C_4H_4N group couples on a metal atom through a C−Pb bond, are much higher in energy than isomer I. The other initial structures collapse to these geometries during the optimization. For isomers of neutral $Pb_2C_4H_4N$, their energies are very close and the difference is about 0.1 eV.

For anion $Pb_3C_4H_4N^-$, there exist two lowest energy structures (I and II) with C_{2v} symmetry, in which the C_4H_4N group couples on a metal atom through an N−Pb bond. The C_4H_4N plane is perpendicular to the Pb_3 plane in isomer I, and is in the same plane with the Pb_3 plane in isomer II. Isomer III, in which the linear Pb_3 cluster couples on the C_4H_4N group through an N−Pb bond, has much higher energy than isomer I. The ortho-isomer (IV) and para-isomer (V) of anion $Pb_3C_4H_4N^-$, in which the C_4H_4N group couples on a metal atom through a C−Pb bond, are also higher in energy than isomers I and II. For isomers I, II, IV, and V of neutral $Pb_3C_4H_4N$, their energies are very close and the difference is about 0.1 eV. However, isomer III has higher energy, and the difference is about 0.8 eV.

From above, we can see that the lowest energy structures of $Pb_mC_4H_4N^-$ ($m = 1-3$) complexes are the isomers in which the C_4H_4N group couples on metal clusters through the N−Pb bond. Blank et al.[40] studied the photodissociation of pyrrole and got the dissociation energy (D0): D0(N−H) = 88 ± 2 kcal/mol, D0(C−H) = 112.5 ± 1 kcal/mol. Theoretical studies also show that N−H bond activation is both kinetically and thermodynamically preferred to C−H activation.[41,42] So for the reaction of lead anionic cluster with C_4H_5N, the most possible way is that Pb_m clusters replace the H atom of the N−H bond and bind the C_4H_4N group through an N−Pb bond to form $Pb_mC_4H_4N^-$ complexes. The electronegativity of the N atom is larger than that of the C atom,[50] and the N atom has stronger attraction for the valence electrons than the C atom. For $Pb_mC_4H_4N^-$ complexes, the N atom has stronger attraction for the valence electrons of the Pb_m cluster. Therefore, the EAs of $Pb_mC_4H_4N$ complexes are higher than those of $Pb_mC_6H_5$, $Pb_mC_5H_4N$, and $Pb_mC_4H_3O$ complexes.

4.4. Assignments of the Complex Structures. In the following, we will confirm the structures of $Pb_mC_4H_4N^-$ ($m = 1-3$) by the help of relativistic DFT. The assignment of the most possible structures of $Pb_mC_4H_4N^-$ is given on the basis of relative energies, and comparisons between the theoretically calculated DOS and the experimental PES spectra. This method of structural assignment has been widely used on cluster studies.[48,51−53] EA is calculated as the difference between the total energies of the neutral and anion at their respective optimized structures. The theoretical DOS is shifted by setting the HOMO level of the spectra to give the negative of DOS value for the complex. This is called theoretically generalized Koopman theorem (GKT)[54]—shifted DOS.[55] The comparisons of theoretical results with the experimental PES spectra of $Pb_mC_4H_4N^-$ are shown in Figures 5−7. Here the DOS is plotted as the stick spectrum in Figures 5−7 by aligning the HOMO level of anions with the threshold peak, instead of the fitted DOS spectra.

4.4.1. $PbC_4H_4N^-$. In Table 2, it is clear that the planar structure with C_{2v} symmetry is the lowest energy structure of neutral PbC_4H_4N and anion $PbC_4H_4N^-$, in which the C_4H_4N group couples on the lead atom through the Pb−N bond, and is considered as in the ground state. The energy difference between the neutral and anionic structures corresponds to the calculated EA listed in Table 2. The calculated EA of PbC_4H_4N by the relativistic DFT is 1.61 eV. It is in good agreement with the experimental results of 1.65 eV. As shown in Figure 5, the energy gap between the HOMO levels in the DOS spectrum

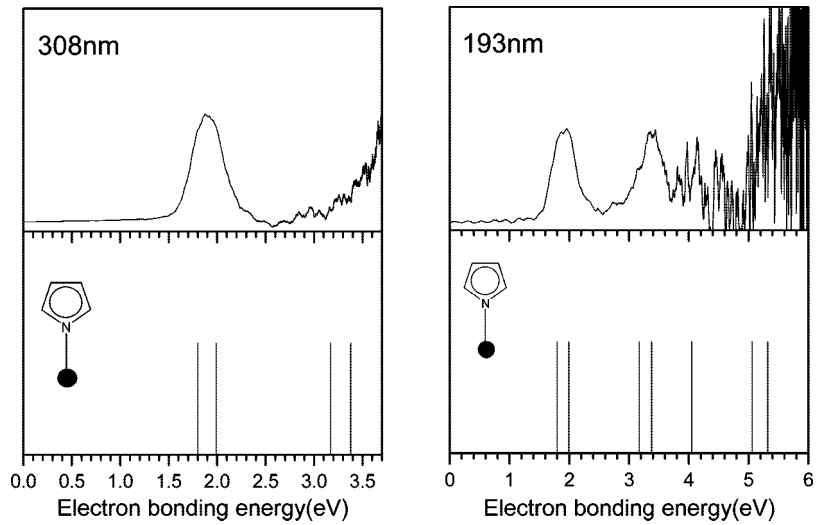

Figure 5. The comparison between PES spectra at 308 and 193 nm photon with theoretical generalized Koopman theorem-shifted DOS for structure I of the $PbC_4H_4N^-$ complex.

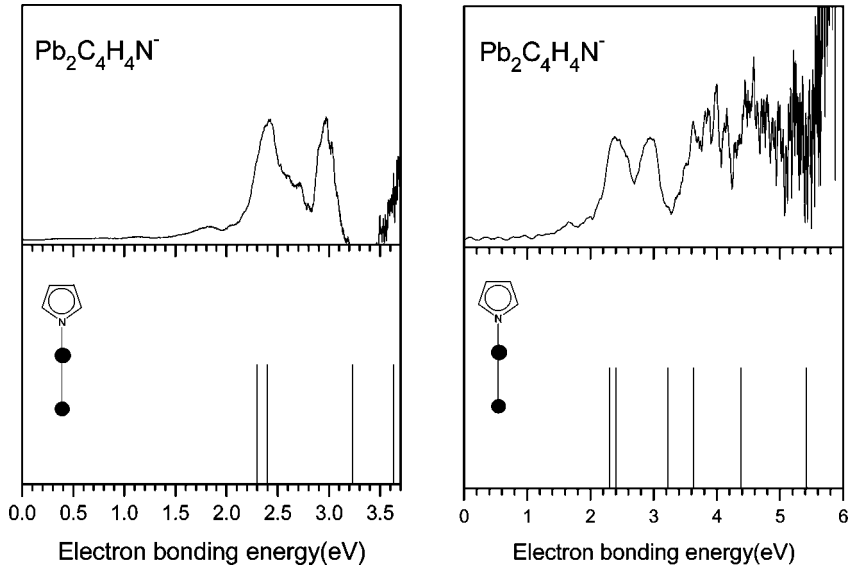

Figure 6. The comparison between PES spectra at 308 and 193 nm photon with theoretical generalized Koopman theorem-shifted DOS for structure I of $Pb_2C_4H_4N^-$.

agrees reasonably well with the experimental PES spectrum. Thus we suggest that isomer I is the ground state of the anion, which contributes to the measured PES spectrum

4.4.2. $Pb_2C_4H_4N^-$. For anionic complexes $Pb_2C_4H_4N^-$, the planar structure (I) with C_{2v} symmetry, in which the C_4H_4N group couples on the Pb_2 cluster through the Pb−N bond, is the lowest energy structure. And also the calculated EA of $Pb_2C_4H_4N$ by the relativistic DFT is 2.26 eV, which is in good agreement with the experimental results of 2.21 eV. As shown in Figure 6, the energy gap between the HOMO levels in the DOS spectrum agrees reasonably well with the experimental PES spectrum. This indicates that the planar structure (I) contributes to the measured PES spectrum.

4.4.3. $Pb_3C_4H_4N^-$. The calculations show that the possible structures of $Pb_3C_4H_4N^-$ are isomer I, II, and III, with EA = 2.57, 2.68, and 2.53 eV, respectively. They are all close to the experimental result of 2.41 eV. The lowest energy structures are isomers I and II with C_{2v} symmetry (the difference is 0.09 eV), in which the C_4H_4N group couples on a metal atom through an N−Pb bond. The isomer III has more energy than isomers I and II. And the three calculated DOS spectra of structures I, II, and III are compared with the experimental PES spectrum as shown in Figure 7. It can be concluded that isomers I and II match the experimental result well and isomer III has some difference from the experimental one. So we support that isomers I and II are both presented in the product $Pb_3C_4H_4N^-$.

4.5. Orbital Composition and Bonding. We have also analyzed the orbital compositions for the most stable anion complexes. The MO pictures from the calculated $Pb_mC_4H_4N^-$ ($m = 1-3$) are given in Figure 8. The molecular orbital pictures for C_4H_4N, Pb_2, and Pb_3 fragments are shown in Figure 9.

For $PbC_4H_4N^-$, it is an open-shell structure that has two unpaired electrons. The HOMO and HOMO-1 are mostly from the $6p_x$ and $6p_y$ of Pb atoms, and the energy gap is very small, corresponding to the first peak of the PES spectrum (shown in Figure 5). The HOMO-2 and HOMO-3 are from the C_4H_4N part (shown in Figure 9), and the HOMO-2 and HOMO-3 correspond to the second peak of the PES spectrum (shown in Figure 5). They are nonbonding MOs for the Pb−C part. The HOMO-4 (10A1) is formed by interaction from 6s and $6p_z$ of the Pb atom with 9a1 of C_4H_4N (mainly formed with N: $2p_z$), and it is a σ MO for the Pb−N part. Therefore, the Pb atom

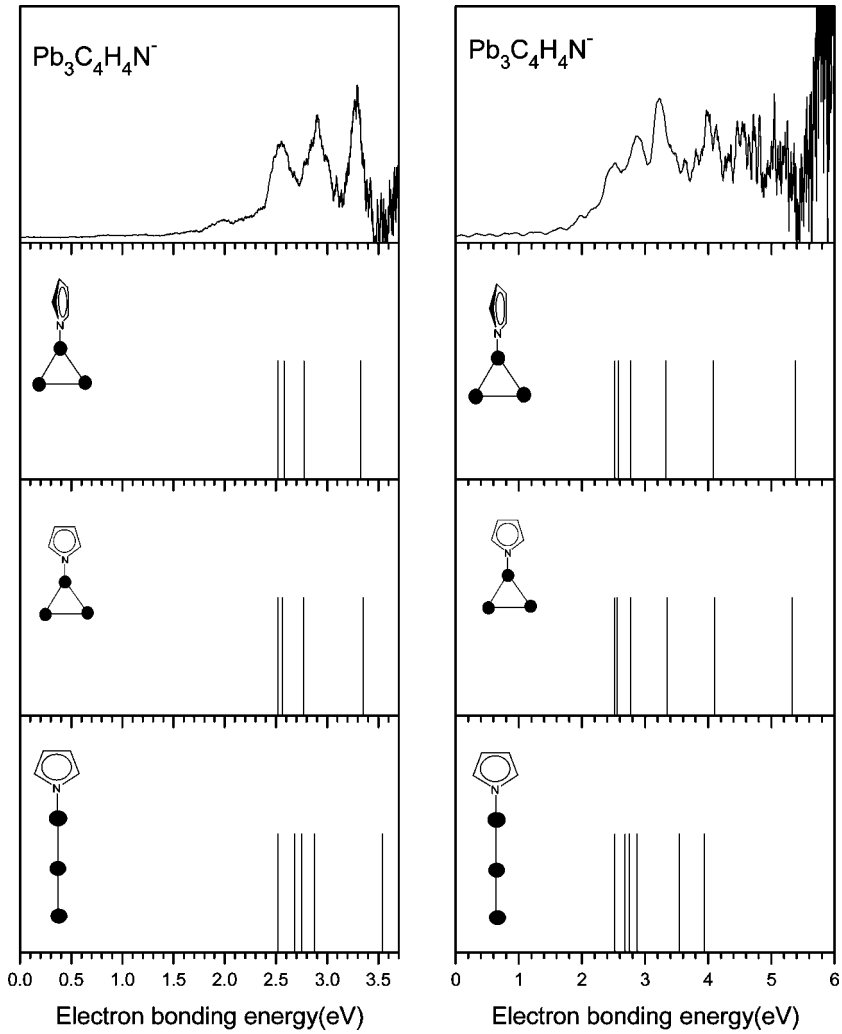

Figure 7. The comparison between PES spectra at 308 and 193 nm photon with theoretical generalized Koopman theorem-shifted DOS for structures I, II, and III of $Pb_3C_4H_4N^-$.

and the C_4H_4N group bind together by the σ bond, in which 6s and $6p_z$ orbits of the Pb atom hybridize and then bond with the $2p_z$ orbit of the N atom.

As for $Pb_2C_4H_4N^-$, the HOMO is mostly from the $6p_x$ interaction of the two Pb atoms and HOMO-1 is mostly from the $6p_y$ interaction of the two Pb atoms. The two MOs are local π-type bonds between Pb and Pb, and the energy gap is very small, corresponding to the first peak of the PES spectrum (shown in Figure 6). The HOMO-2 and HOMO-3 are from the C_4H_4N part (shown in Figure 9), corresponding to the second and third peaks of the PES spectrum (shown in Figure 6). They are nonbonding MOs for the Pb−C part. The HOMO-4 (11A1) is formed by interaction from 6s and $6p_z$ of the Pb atom with 9a1 of C_4H_4N (mainly formed with N: $2p_z$), and it is a σ MO for the Pb−N part. Therefore, the Pb_2 cluster and the C_4H_4N group bind together by the σ bond, in which 6s and $6p_z$ orbits of the Pb atom hybridize and then bond with the $2p_z$ orbit of the N atom.

There are two possible isomeric structures I and II of $Pb_3C_4H_4N^-$ as shown above, and their MOs near HOMO are similar. Their MO pictures are shown in Figure 8, parts c and d. As an example, the MO analysis of structure I in Figure 8c only is given below. The HOMO and HOMO-1 are mostly the local σ MOs between Pb atoms (shown in Figure 8c) and the energy gap is very small, corresponding to the first peak of the PES spectrum (shown in Figure 7). HOMO-2 is mostly the local π MOs between Pb atoms, corresponding to the second peak of the PES spectrum. The HOMO-3 and HOMO-4 are from the C_4H_4N part (shown in Figure 9), corresponding to the third and fourth peaks of the PES spectrum. Only the HOMO-5 is a σ MO for the Pb−N part, and the inner MOs are nonbonding MOs for the Pb−N part. So we can confirm that the Pb_3 cluster connects with the C_4H_4N group by the Pb−N σ bond in $Pb_3C_4H_4N^-$.

The theoretical calculations confirm that an excess electron on the anions attaches to the Pb clusters. For each of the $Pb_mC_4H_4N^-$ complexes, there exists only one σ MO for the Pb−N part, which can be evidence that the C_4H_4N group binds on the lead clusters through the Pb−N σ bond. This interaction can also influence the energy level of the outer MOs. Thus the threshold electron energy of $Pb_mC_4H_4N^-$ complexes is higher than those of $Pb_mC_6H_5^-$, $Pb_mC_5H_4N^-$, and $Pb_mC_4H_3O^-$ complexes.

5. Conclusions

The reactions between lead vapor generated by laser ablation and different aromatic molecules (C_6H_6, C_5H_5N, C_4H_4O, or C_4H_5N) seeded in argon carrier gas are studied by a reflectron time-of-flight mass spectrometer (RTOF-MS). The EAs of the dominant products $Pb_mC_6H_5$, $Pb_mC_5H_4N$ ($m = 1-4$), and $Pb_mC_4H_3O$, $Pb_mC_4H_4N$ ($m = 1-4$) dehydrogenated complexes are obtained from the photoelectron spectra with 308 and 193

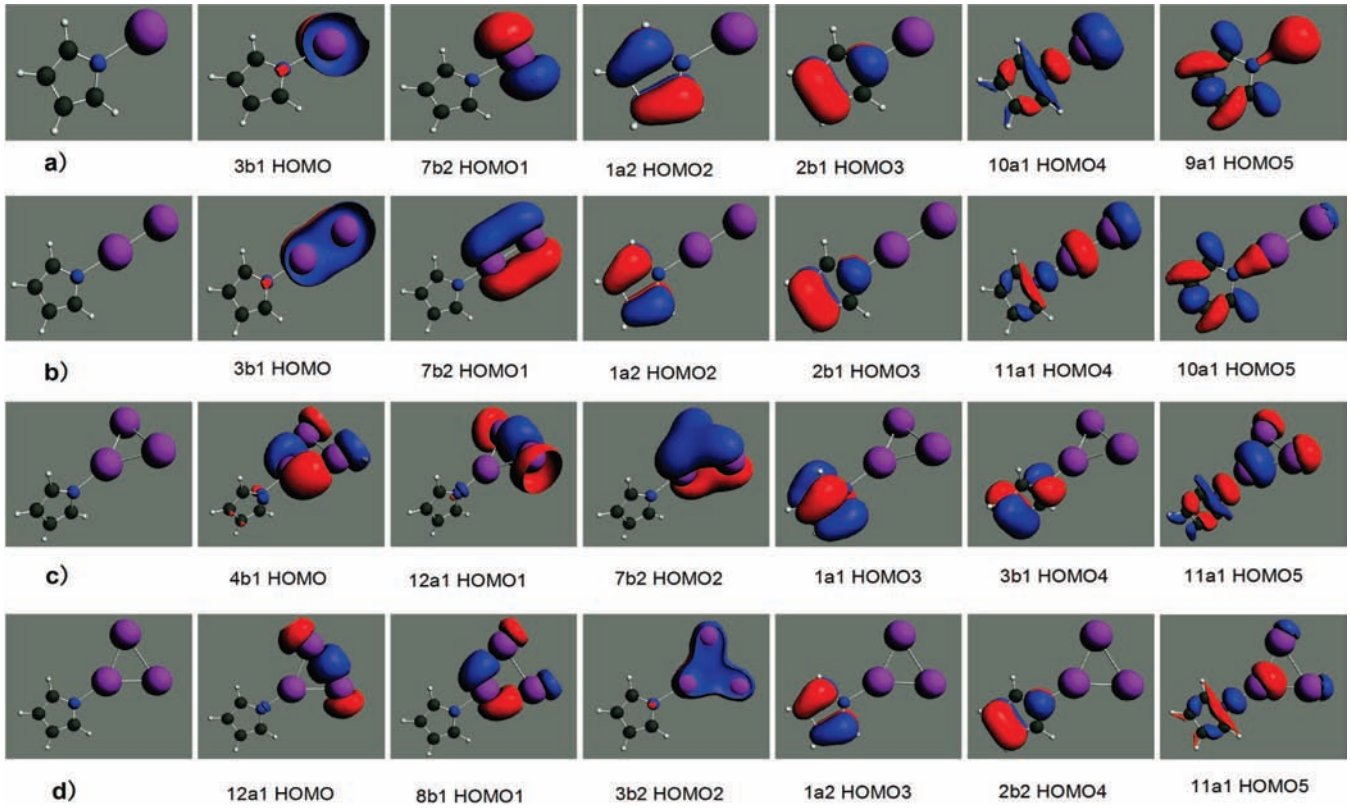

Figure 8. Molecular orbital drawings for (a) $PbC_4H_4N^-$, (b) $Pb_2C_4H_4N^-$, (c) $Pb_3C_4H_4N^-$ (structure I,) and (d) $Pb_3C_4H_4N^-$ (structure II). The first drawing in each row is the coordinate sketch of the cluster complex corresponding to its molecular orbital drawing.

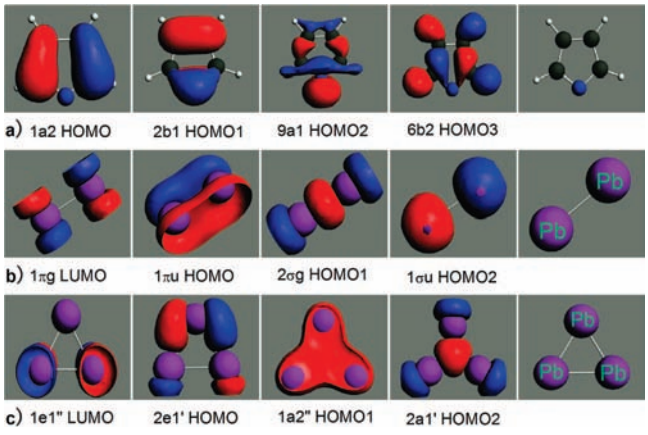

Figure 9. Molecular orbital drawings for fragments (a) C_4H_4N, (b) Pb_2, and (c) Pb_3. The last drawing in each row is the coordinate sketch of the cluster complex corresponding to its molecular orbital drawing.

nm photon, respectively. It is found that the EAs of $Pb_mC_4H_4N$ are higher than those of $Pb_mC_6H_5$, $Pb_mC_5H_4N$, and $Pb_mC_4H_3O$ ($m = 1-3$), which shows that the C_4H_4N group has stronger interaction with Pb_m clusters to result in the electron detachment threshold of $Pb_mC_4H_4N^-$ complexes being higher than those of the others.

For each of $Pb_mC_4H_4N^-$, the theoretical EAs are in good agreement with EAs from PES spectra. By comparison of the experimentally measured PES and DOS calculated by the relativistic DFT, we assigned the most possible structures. All the assigned structures of $Pb_mC_4H_4N^-$ ($m = 1-3$) are the lowest energy structures with C_{2v} symmetry, and the C_4H_4N group binds on lead clusters through the Pb−N σ bond. For $Pb_3C_4H_4N^-$, the calculated DOS of the two lower energy structures all match with the experimental spectrum well, suggesting that the PES spectrum of $Pb_3C_4H_4N^-$ is contributed from structures I and II. Furthermore, the MOs analysis of these species shows that the theoretical calculations are in good agreement with the experimental PES spectra.

Acknowledgment. We gratefully acknowledge the support of the National Natural Science Foundation of China under Grant Nos. 20203020 and 20433080. We are grateful to Dr. Weijun Zheng for his advice on this paper.

References and Notes

(1) Hoshino, K.; Kurikawa, T.; Takeda, H.; Nakajima, A.; Kaya, K. *J. Phys. Chem.* **1995**, *99*, 3053.
(2) Kurikawa, T.; Hirano, M.; Takeda, H.; Yagi, K.; Hoshino, K.; Nakajima, A.; Kaya, K. *J. Phys. Chem.* **1995**, *99*, 16248.
(3) Kurikawa, T.; Takeda, H.; Hirano, M.; Judai, K.; Arita, T.; Nagao, S.; Nakajima, A.; Kaya, K. *Organometallics* **1999**, *18*, 1430.
(4) Xing, X. P.; Tian, Z. X.; Liu, H. T.; Tang, Z. C. *J. Phys. Chem. A* **2003**, *107*, 8484.
(5) Miyajima, K.; Yabushita, S.; Knickelbein, M. B.; Nakajima, A. *J. Am. Chem. Soc.* **2007**, *129*, 8473.
(6) Luttgens, G.; Pontius, N.; Friedrich, C.; Klingeler, R.; Bechthold, P. S.; Neeb, M.; Eberhardt, W. *J. Chem. Phys.* **2001**, *114*, 8414.
(7) Jaeger, T. D.; Duncan, M. A. *Int. J. Mass Spectrom.* **2005**, *241*, 165.
(8) Sohnlein, B. R.; Lei, Y. X.; Yang, D. S. *J. Chem. Phys.* **2007**, 127.
(9) Lyon, J. T.; Andrews, L. *J. Phys. Chem. A* **2006**, *110*, 7806.
(10) Sohnlein, B. R.; Yang, D. S. *J. Chem. Phys.* **2006**, 124.
(11) Jaeger, T. D.; Duncan, M. A. *J. Phys. Chem. A* **2005**, *109*, 3311.
(12) Zheng, W. J.; Nilles, J. M.; Thomas, O. C.; Bowen, K. H. *J. Chem. Phys.* **2005**, 122.
(13) Zheng, W. J.; Nilles, J. M.; Thomas, O. C.; Bowen, K. H. *Chem. Phys. Lett.* **2005**, *401*, 266.
(14) Gerhards, M.; Thomas, O. C.; Nilles, J. M.; Zheng, W. J.; Bowen, K. H. *J. Chem. Phys.* **2002**, *116*, 10247.
(15) Kah Chun Lau, M. D. R. P. *Int. J. Quantum Chem.* **2005**, *102*, 656.
(16) Rao, B. K.; Jena, P. *J. Chem. Phys.* **2002**, *117*, 5234.
(17) Wu, D. Y.; Ren, B.; Jiang, Y. X.; Xu, X.; Tian, Z. Q. *J. Phys. Chem. A* **2002**, *106*, 9042.

(18) Kandalam, A. K.; Rao, B. K.; Jena, P.; Pandey, R. *J. Chem. Phys.* **2004**, *120*, 10414.
(19) BelBruno, J. J. *Surf. Sci.* **2005**, *577*, 167.
(20) Rabilloud, F. *J. Chem. Phys.* **2005**, *122*, 134303.
(21) Jaeger, T. D.; van Heijnsbergen, D.; Klippenstein, S. J.; von Helden, G.; Meijer, G.; Duncan, M. A. *J. Am. Chem. Soc.* **2004**, *126*, 10981.
(22) Miyajima, K.; Muraoka, K.; Hashimoto, M.; Yasuike, T.; Yabushita, S.; Nakajima, A.; Kaya, K. *J. Phys. Chem. A* **2002**, *106*, 10777.
(23) Froudakis, G. E.; Andriotis, A. N.; Menon, M. *Chem. Phys. Lett.* **2001**, *350*, 393.
(24) Sahnoun, R.; Mijoule, C. *J. Phys. Chem. A* **2001**, *105*, 6176.
(25) Pandey, R.; Rao, B. K.; Jena, P.; Blanco, M. A. *J. Am. Chem. Soc.* **2001**, *123*, 3799.
(26) Rahman, M. M.; Muhida, R.; Dy, E. S.; Mozo, R.; Kasai, H. *J. Phys. Soc. Jpn.* **2006**, 75.
(27) Kua, J.; Tomlin, K. M. *J. Phys. Chem. A* **2006**, *110*, 11988.
(28) Rao, B. K.; Jena, P. *J. Chem. Phys.* **2002**, *116*, 1343.
(29) Xing, X. P.; Liu, H. T.; Tang, Z. C. *Physchemcomm* **2003**, *6*, 32.
(30) Sun, S. T.; Xing, X. P.; Liu, H. T.; Tang, Z. C. *J. Phys. Chem. A* **2005**, *109*, 11742.
(31) Liu, H. T.; Xing, X. P.; Sun, S. T.; Gao, Z.; Tang, Z. C. *J. Phys. Chem. A* **2006**, *110*, 8688.
(32) Dai, D. G.; Balasubramanian, K. *Chem. Phys. Lett.* **1997**, *271*, 118.
(33) Zhao, C. Y.; Balasubramanian, K. *J. Chem. Phys.* **2002**, *116*, 10287.
(34) Tang, I. N.; Castleman, A. W., Jr *J. Chem. Phys.* **1972**, *57*, 3638.
(35) Guo, B. C.; Purnell, J. W.; Castleman, A. W. *Chem. Phys. Lett.* **1990**, *168*, 155.
(36) Pozherskii, A. F.; Soldatenkov, A. T.; Katritzky, A. R. *Heterocycles in Life and Society*; Wiley: New York, 1997.
(37) Katritzky, A. R. *Handbook of Heterocyclic Chemistry*, 2nd ed.; Elsevier Science Ltd.: New York, 2000.
(38) Wiberg, K. *Aromaticity and Its Chemical Manifestations, Pauling's Legacy: Modern Modelling of the Chemical Bond*; Elsevier: Amsterdam, The Netherlands, 1999; Vol. 6.
(39) Elnagdi, M. H.; Al-Awdi, N.; Erian, A. W. *Comprehensive Heterocyclic Chemistry*; Pergamon Press: London, UK,1996.
(40) Blank, D. A.; North, S. W.; Lee, Y. T. *Chem. Phys.* **1994**, *187*, 35.
(41) Feng, Y.; Wang, J. T.; Liu, L.; Guo, Q. X. *J. Phys. Org. Chem.* **2003**, *16*, 883.
(42) Barckholtz, C.; Barckholtz, T. A.; Hadad, C. M. *J. Am. Chem. Soc.* **1999**, *121*, 491.
(43) Xing, X. P.; Tian, Z. X.; Liu, P.; Gao, Z.; Zhu, Q.; Tang, Z. C. *Chin. J. Chem. Phys.* **2002**, *15*, 83.
(44) Xing, X. P.; Liu, H. T.; Sun, S. T.; Cao, Y. L.; Tang, Z. C. *Chin. J. Chem. Phys* **2004**, *17*, 321.
(45) Perdew, J. P.; Wang, Y. *Phys. Rev. B* **1992**, *45*, 13244.
(46) van Lenthe, E.; Baerends, E. J.; Snijders, J. G. *J. Chem. Phys.* **1993**, *99*, 4597.
(47) Vrije Universiteit, ADF2005,SCM, Theoretical Chemistry, Amsterdam, The Netherlands (www.scm.com).
(48) Li, J.; Li, X.; Zhai, H.-J.; Wang, L.-S. *Science* **2003**, *299*, 864.
(49) Liu, H. T.; Sun, S. T.; Xing, X. P.; Tang, Z. C. *Rapid Commun. Mass Spectrom.* **2006**, *20*, 1899.
(50) Dean., J. A. *Lange's Handbook of Chemistry*; McGraw-Hill: New York, 1999.
(51) Li, X.; Kiran, B.; Li, J.; Zhai, H. J.; Wang, L. S. *Angew. Chem.* **2002**, *41*, 4786.
(52) Wang, L. S.; Wang, X. B.; Wu, H. B.; Cheng, H. S. *J. Am. Chem. Soc.* **1998**, *120*, 6556.
(53) Häkinen, H.; Moseler, M.; Landman, U. *Phys. Rev. Lett.* **2002**, *89*, 033401.
(54) Tozer, D. J.; Handy, N. C. *J. Chem. Phys.* **1998**, *108*, 2545.
(55) Hakkinen, H.; Yoon, B.; Landman, U.; Li, X.; Zhai, H. J.; Wang, L. S. *J. Phys. Chem. A* **2003**, *107*, 6168.

JP805837B